Lawrence Berkeley National Laboratory
LBL Publications

Title
On-site interband excitations in resonant inelastic x-ray scattering from Cu2O

Permalink
https://escholarship.org/uc/item/3kq8415v

Authors
Hu, J. P.
Payne, D. J.
Egdell, R. G.
et al.

Publication Date
2008-04-15

eScholarship.org Powered by the California Digital Library
University of California

On-site interband excitations in resonant inelastic X-ray scattering from Cu_2O.

J.P. Hu, D. J. Payne, R. G. Egdell*,

Department of Chemistry, Inorganic Chemistry Laboratory, South Parks Road,

Oxford OX1 3QR, UK.

P.-A. Glans, T. Learmonth, K.E. Smith

Department of Physics, Boston University, 590 Commonwealth Ave., Boston, MA 02215, USA

J. Guo

Advanced Light Source, Lawrence Berkeley National Laboratory, Berkeley, CA 94720, USA

N.M. Harrison,

STFC, Daresbury Laboratory, Warrington, Cheshire, WA4 4AD, UK and

Department of Chemistry, Imperial College, London, SW7 2AZ, UK.

Abstract.

The electronic structure of cuprite (Cu_2O) has been studied by high resolution X-ray photoemission (XPS) and X-ray absorption (XAS) and resonant X-ray emission spectroscopies (XES) supported by band structure calculations using a hybrid exchange approximation to density functional theory. A pronounced loss feature at about 4.5 eV due to on-site interband excitation has been identified in resonant inelastic X-ray scattering from Cu_2O close to the L_3 (Cu $2p_{3/2}$) core threshold. Although Cu_2O nominally has a filled upper valence band of Cu 3d states and an empty conduction band of Cu 4s states, the band structure calculations show that there is substantial 3d character in the conduction band and that the inelastic loss is dominated by onsite 3d to 3d excitation conforming to the selection rule $\Delta l = 0$ rather than 3d to 4s transitions with $\Delta l = -2$. However unlike in previous work these transitions do not arise from ligand field splitting of the Cu 3d states but rather from onsite 3d-4s hybridisation which introduces 3d character into the conduction band. Comparison between XPS, XES and XAS data shows that Cu L_3 XAS is dominated by a core exciton lying 0.65 eV below the bottom of the conduction band and that inelastic scattering is only observed for photon energies below that required to excite the core electron into the conduction band.

I. INTRODUCTION.

There is a growing interest in the development of electronic and optoelectronic devices based on oxides which are transparent in the visible region but which can be doped to induce a high electrical conductivity. Most of the established transparent conducting oxides (TCOS) of this sort are n-type materials[1]. This includes the prototype TCOs SnO_2, In_2O_3 and ZnO. It has proved very difficult to develop reproducible strategies for the p-type doping of these materials.[2-4] However, exploitation of transparent conducting oxides in devices such as UV diodes will only become possible if suitable wide gap oxides that can be doped *p*-type can be developed. In the classical n-type TCOs, the top of the valence band is composed of O 2p states and it is not surprising that it is difficult to introduce holes into these bands: in chemical terms one is attempting to oxidise oxygen. However in cuprite (Cu_2O) the upper valence band states are of dominant Cu 3d atomic character and introduction of holes involves oxidation of $3d^{10}$ Cu(I) to $3d^9$ Cu(II). This process is chemically tractable and Cu_2O is indeed a *p*-type semiconductor. The electronic bandgap in Cu_2O is 2.17eV[5] and is therefore too small for application in TCO devices. However, the bandgaps in many ternary Cu(I) oxides are much bigger than in the parent Cu_2O. This has allowed development of new families of *p*-type conducting ternary Cu(I) oxides that are transparent in the visible region.[6-13] Cu_2O itself has emerged as a *p*-type host for doping with magnetic ions in order to induce room temperature dilute semiconductor ferromagnetism.[14-17] The recent interest in the functional properties of Cu(I) oxides has prompted us to revisit the electronic structure of Cu_2O. The main focus of the present paper is investigation of the nature of electronic excitations in Cu_2O found in resonant inelastic X-ray scattering (RIXS) at the Cu L_3 edge. Previous photon excited X-ray emission (XES) studies of Cu_2O have been restricted to the Cu K[18,19] and Cu $M_{3,2}$[20] edges. In both cases resolution was limited by very pronounced lifetime broadening (>1.5eV) of

the core hole and no attempt was made to study resonant X-ray scattering. Elsewhere electron beam excited Cu L and O K emission spectra were reported many years ago[21], but again with poor overall effective resolution and with no possibility to study resonant emission. The discovery of pronounced resonant inelastic X-ray scattering at the Cu L_3 edge in the current study prompted re-examination of high resolution X-ray photoemission (XPS) and X-ray absorption (XAS) spectra of Cu_2O. In contrast to previous valence region XPS studies[22-23], particular care was taken to establish the position of the Fermi level relative to the valence band edge. This then enabled exploration of the relationship between core level binding energies in XPS and the energies of features in XAS and XES. It is shown that the Cu L_3 absorption spectrum[24-26] is dominated by a core-hole exciton that lies 0.65 eV below the bottom of the conduction band. The experimental work is supported by bandstructure calculations using a hybrid exchange approximation to density functional theory that gives an accurate first principles description of the bulk bandgap. The combined experimental and theoretical study leads to the identification of a general mechanism for inelastic X-ray scattering in Cu(I) compounds.

The primitive cubic structure of Cu_2O belongs to the space group O_h^4 and is based on a body centred cubic array of oxygen ions with Cu ions occupying half the sites between adjacent oxygen ions. The O ions are found at (0,0,0) and (1/2,1/2,1/2) and the Cu ions at (1/4,1/4,1/4), (3/4,1/4,3/4), (1/4,3/4,3/4) and (3/4,3/4,1/4), giving two formula units per cell. The structure can alternatively be described in terms of two interpenetrating anti-SiO_2 cristabolite nets.[27] In this structure the Cu ions occupy sites with linear coordination by two O ions, although due to a staggered arrangement of the three additional Cu ions bonded to these two oxygen ions, the local site symmetry is D_{3d}. In addition the separation between adjacent Cu ions in the two different nets is quite small (~3.02 Å) allowing significant interaction between them. This in turn influences the

width of the valence band. The O ions are surrounded by four copper ions in a tetrahedral arrangement. The unusual structure is associated with negative thermal expansion.[28]

In the simplest ionic model description Cu_2O is a d^{10} oxide. An upper valence band of filled Cu 3d states sits above a band of filled O 2p states, whilst the bottom of the conduction band is nominally composed of Cu 4s states with empty Cu 4p states at higher energy. In terms of the linear O-Cu-O units, the Cu $3d_{z^2}$ orbitals have σ-like symmetry, the $3d_{xz}$ and $3d_{yz}$ orbitals π-like symmetry and the $3d_{xy}$ and $3d_{x^2-y^2}$ orbitals δ-like symmetry. Thus O 2p orbitals can mix with Cu $3d_{z^2}$ via strong σ overlap and with $3d_{xz}$ and $3d_{yz}$ via weaker π interactions. However the $3d_{xy}$ and $3d_{x^2-y^2}$ orbitals must remain localised on Cu as there are no orbitals on oxygen of the correct δ symmetry for covalent mixing. Within this description, the lowest energy interband transitions of Cu_2O are basically from a filled upper valence band of Cu 3d states (mixed to some extent with O 2p states) into an empty conduction band of Cu 4s states. Interband excitations are therefore onsite transitions conforming to a change in angular momentum $\Delta l = -2$, which makes the transitions allowed in inelastic X-ray Raman scattering where the atomic selection rule is $\Delta l = 0, \pm 2$. However the band calculations show that due to extensive mutual mixing between O 2p, Cu 3d and Cu 4s states this simple description must be modified. It transpires that onsite 4s-3d hybridisation introduces significant Cu 3d character into the conduction band so that even though Cu_2O is nominally a $3d^{10}$ oxide, the interband transitions have significant 3d to 3d character and thus satisfy $\Delta l = 0$. This allowed channel is mediated exclusively by matrix elements between core Cu 2p states and Cu 3d states and does not involve matrix elements between Cu 2p and Cu 4s states. Since the former are much bigger[26,29] the energy loss is dominated by the full and empty Cu 3d partial densities of states.

II. ELECTRONIC STRUCTURE CALCULATIONS

The calculations presented have been performed using the CRYSTAL06 software.[30] Electronic exchange and correlation were approximated using the hybrid exchange formalism which has previous been demonstrated to provide a reliable description of the ground state electronic structure in copper oxides[31] and, of particular relevance to the current study, of the nature and value of the band gap in a wide variety of materials.[32] The most significant numerical approximation is the expansion of the crystalline orbitals in a basis set consisting of a linear combination of atom centered Gaussian orbitals. High quality all-electron basis sets used in previous studies[33,34] were adopted to describe the Cu and O ions and the outermost exponents re-optimized *in situ.* This resulted in the use of a quadruple valence set for the Cu-ion of structure 864111-D31 with outer sp exponents (in a_0^{-2}) of 1.582, 0.559 and 0.15 and outer d-exponent of 0.430. The triple valence O basis set, 8411D, had outer sp-exponents of 0.425 and 0.125 with a d-exponent of 0.5. The Coulomb and exchange series were truncated using overlap criteria documented elsewhere[30] (strict tolerances of 7 7 7 7 14 were adopted) and the exchange correlation potentials and energy were integrated numerically on an atom centered grid of points containing approximated 2500 symmetry irreducible points per atom (the XLGRID option[30]). Finally k-space integration was performed on a Pack-Monkhurst grid defined by a shrinking factor of 8 which contained 59 symmetry irreducible points.

III. EXPERIMENT

Cu_2O was prepared by decomposing CuO under flowing Ar at 900°C. The high purity powder sample was pressed into discs between tungsten carbide dies and further sinterd under Ar at 900°C to give robust ceramic discs. Phase purity was confirmed by X-ray powder diffraction.

High-resolution X ray photoemission spectra were measured in a Scienta ESCA 300 spectrometer. This incorporates a rotating anode Al Kα ($h\nu$ = 1486.6 eV) X-ray source, a 7 crystal X-ray monochromator and a 300mm mean radius spherical sector electron energy analyser with parallel electron detection system. The X-ray source was run with 200 mA emission current and 14 kV anode bias, whilst the analyser operated at 150 eV pass energy with 0.8mm slits. Gaussian convolution of the analyser resolution with a linewidth of 260 meV for the X-ray source gives an effective instrument resolution of 350 meV. The Cu_2O sample was cleaned by a surface science recipe which involved bombardment with Ar ions, followed by annealing in order to heal ion beam damage.[35-37] Following bombardment with 2.5 kV Ar ions for 15 minutes followed by annealing in UHV (5×10^{-9} mbar) at first 550°C and then 650°C for 1 hour, the O 1s core line assumed a narrow profile (full width at half maximum height 0.66 eV) with a symmetric shape and a without high binding energy shoulder due to surface adsorbates. In addition satellites due to CuO were eliminated from Cu 2p core level spectra. Finally the Cu 2p to O 1s intensity ratio after correction for atomic sensitivity factors[38] assumed a value of 1.54, which is within the range found for ordered single crystal $Cu_2O(100)$ surfaces with Cu terminated reconstructions.[35,36] The C 1s to O1s intensity ratio was reduced to below 1/100. Binding energies are referenced to the Fermi energy of a silver sample regularly used to calibrate the spectrometer.

X-ray absorption and emission spectra were measured at beamline 7.0.1 at the Advanced Light Source (ALS), Lawrence Berkeley National Laboratory. This beamline is equipped with a spherical grating monochromator.[39] Emission spectra were recorded using a Nordgren-type grazing-incidence spherical grating spectrometer.[40] For resonant emission experiments, the beamline was set to have an energy resolution of 500 meV at the O K edge and 1 eV at the Cu L_3 edge, and the emission spectrometer was set to have a resolution of 350 meV for O K and 750 meV for Cu L_3 edge spectra. Absorption spectra were measured in total fluorescence yield (TFY) and total electron yield (TEY) modes. For the absorption measurements, the beamline resolution was set to 200 meV for the O K edge and to 1 eV for the Cu L_3 edge. The absorption spectra were normalised to a reference current from a clean gold mesh positioned in the path of the photon beam. The energy scale of the O K absorption spectra was calibrated relative to the O K absorption spectrum of NiO and the Cu L emission spectra were calibrated relative to the L absorption spectrum of Cu metal. The O K-edge emission spectra were calibrated to Zn $L\alpha_{1,2}$ and $L\beta_1$ emission lines of Zn metal in second order, and the Cu L-edge emission spectra were calibrated to relative to metallic Cu $L\alpha_{1,2}$ and $L\beta_1$ emission spectra measured in first order. The consistency of the calibrations in XPS and XES is demonstrated by the fact that the peak maximum in non-resonant Cu L_3 XES (corresponding to the position of the peak maximum in the Cu 3d partial density of states relative to the Cu $2p_{3/2}$ core hole) is at 929.4 eV ± 0.2 eV whilst the separation between the Cu$2p_{3/2}$ core level and valence band peak maxima (the latter again corresponding to the position of the peak maximum in the Cu 3d partial density of states) in XPS is 929.5 eV ± 0.1 eV .

IV. RESULTS AND DISCUSSION

A. The electronic density of states.

The full and partial densities of states derived from the bandstructure calculations are shown in figure 1. The occupied full and empty densities of states are in broad general agreement with previous work[41-49] although with exception of the semiempirical calculations of Robertson[43] and the self interaction corrected LDA calculation of Filippetti *et al.*[48] the present calculations reproduce the experimental bandgap and valence band width much better than previously (table 1). In particular earlier density functional calculations[42,44,46] underestimated the bulk band gap whereas a Hartree-Fock calculation[45] dramatically overestimated the gap. The failure of these well-established methods is well known and has been discussed in many previous publications.[32,50] The hybrid method used in the present work introduces an element of Hartree-Fock exchange into the density functional Hamiltonian and has been shown to give accurate predictions of bulk bandgaps for a very wide range of materials.[32]

Looking in more detail at the full and partial densities of states it can be seen that the upper part of the valence band is of dominant Cu 3d atomic character and the lower part is of dominant O 2p character. The lower O 2p states are themselves split into two components *x* and *y*. There is significant covalent mixing of Cu 3d character into both *x* and *y*, although the Cu 3d contribution is slightly stronger in the more tightly component *x*: the Cu 3d / O 2p ratio at the maximum in *x* is 0.32, whereas the ratio at the maximum in *y* is 0.28. The structure in the Cu 3d part of the valence band contains a strong peak labelled *a* in figure 1, which has two subsidiary maxima *a*' and *a*'' on the high binding energy side, together with a weaker peak *b* at lower binding energy and close the top of the valence band. There is in turn covalent mixing of O 2p character into the Cu 3d states. It is however striking that this mixing is much stronger in *b* than in *a*. Thus the O 2p / Cu

3d ratio at the peak maximum in *b* is 0.23 whereas the ratio at the peak maximum in *a* is 0.008. This accords with the qualitative discussion outlined in the introduction which led us to anticipate that states at the top of the valence band should be antibonding and involve mixing between the σ-like Cu $3d_{z^2}$ orbitals and an appropriately symmetrised linear combination of σ-like O 2p orbitals. By contrast the band *a* contains δ-like Cu $3d_{x^2-y^2}$ and Cu $3d_{xy}$ states which cannot mix with O 2p states, as well as the Cu $3d_{xz}$ and Cu $3d_{yz}$ states which can only mix with O 2p states via weak π-type overlap. These qualitative ideas are in agreement with the conclusions of Marksteiner *et al.*[44], who performed a projection of the Cu 3d partial density of states into local σ, π and δ components. This earlier work showed that σ-like Cu $3d_{z^2}$ character was found in band *b* and in band *x*, at the top and bottom of the valence band respectively. In addition Marksteiner *et al.*[44] found that there was also a significant contribution from Cu $3d_{z}^2$ states at the bottom of band *a* in *a''*, which lies between the main O 2p and Cu 3d valence bands. Turning back to discussion of our own calculations we find that in contrast to the simple ionic model description which treats Cu^+ as a $3d^{10}4s^0$ cation, significant Cu 4s character is found in the valence band. Three pronounced maxima are found in the Cu 4s occupied partial density of states at energies corresponding to the peaks *b, a''* and *x*. Two of these maxima (those in *b* and *a"*) in the Cu 4s partial density of states therefore coincide with maxima in the Cu 3d partial density of states, indicating that there is pronounced on-site 3d – 4s hybridisation. This finding is in agreement with qualitative ideas first developed by Orgel[51] that rationalised the linear coordination found for Cu(I) compounds in terms of onsite Cu 3d – Cu 4s mixing. These conclusions are also in accord with very recent LDA+U calculations and angle resolved photoemission measurements which found evidence for a state with mixed Cu 3d and Cu 4s character between the main band of Cu 3d states and the O 2p band.[52] The overall width of the Cu 3d part of the valence band in Cu_2O is

found to be about 4.0 eV in our calculations. This is significantly greater than the value of 2.8 eV for $SrCu_2O_2$ found in a recent calculation using the same hybrid Hamiltonian approach adopted here.[53] This is despite the fact that the next neighbour coordination of Cu by two O ions in a linear arrangement in $SrCu_2O_2$ is similar to that in Cu_2O and the Cu-O bondlengths have almost identical values of 1.85Å (Cu_2O) and 1.84Å ($SrCu_2O_2$). The main difference between the two oxides is in the dimensionality of next nearest neighbour interactions between the Cu $3d^{10}$ shells. In Cu_2O each Cu ion has12 next-nearest Cu neighbours (6 of which belong to the interpenetrating framework) in a 3D arrangement with a Cu-Cu separation of 3.01 Å. In $SrCu_2O_2$ by contrast there are only 2 next nearest Cu neighbours in a linear 2D arrangement, albeit with a reduced Cu-Cu separation of 2.74 Å. The smaller Cu 3d bandwidth in $SrCu_2O_2$ and the associated increase in the bandgap, reflects this difference.

Turning now to the empty density of states in Cu_2O, it can be seen in figure 1 that Cu 4s and Cu 3d states make the strongest contributions to the bottom of the conduction band. At higher energy the Cu 4p contribution becomes dominant. In addition there is a significant O 2p contribution to the conduction band.

B. X-ray photoemission and non-resonant X-ray emission spectra.

Experimental valence band X-ray photoemission spectra of Cu_2O are shown in figure 2 along with O K and Cu L_3 X-ray emission spectra excited under non-resonant conditions well above the core threshold. The photoemission spectrum is compared with the density of states from the bandstructure calculations with the differing partial contributions to the total density of states weighted in proportion to one electron ionisation cross sections computed at $h\nu$ = 1486.6 eV. At this energy the one electron cross section for ionisation of Cu 3d states is a factor of twenty

bigger than the cross section for ionisation of O 2p states.[54] The overall cross section weighted density of states is therefore dominated by the Cu 3d partial density of states. The experimental spectrum is in agreement with the calculation both in terms of the overall shape of the spectral profiles and in terms of the relative intensities of the upper and lower parts of the valence band. In particular much of the intensity in the O 2p region in the lower half of the valence band is a direct reflection of covalent mixing of Cu 3d character into the lower valence band states. However there is a small but significant contribution to the intensity in this region from the O 2p states themselves. Conversely the O K shell X-ray emission spectrum is a direct measure of the O 2p partial density of states. The lower valence band states are the strongest spectral features but again due to covalency there is significant intensity in the upper valence band region. In agreement with the calculations there is however little intensity in the region of the most tightly bound Cu 3d states which dominate the X-ray photoemission spectrum. This reflects the fact that these states have local δ character and cannot therefore mix with O 2p states. Finally the Cu L_3 emission spectrum is a probe the Cu 3d partial density of states but without any O 2p contribution. The spectral profile is similar to the X-ray photoemission spectrum albeit with poorer resolution. However it is noticeable that the lower valence band structure is slightly weaker relative to the Cu 3d maximum than in X-ray photoemission. This is because the O 2p partial density of states makes a small contribution to X-ray photoemission intensity but not to Cu L_2 X-ray emission.

C. X-ray absorption spectra and core lines in X-ray photoemission

O K and Cu $L_{2,3}$ X-ray absorption spectra are shown in figure 3. Both spectra contain a strong and relatively narrow peak close to the absorption threshold with maxima at 532.4 eV and 933.7(5) eV respectively. These energies are in excellent agreement with corresponding values of 933.7 eV and 532.5 eV found by Grioni *et al*.[25] The O K shell absorption spectrum basically mimics the unoccupied O 2p partial density of states. However the strikingly asymmetric lineshape in the threshold peak of the Cu L_3 spectrum is not reproduced by the bandstructure calculations. The spectrum can be regarded as a superposition of an excitonic component at threshold with structure at higher energy that is associated with the empty density of states.[25]

It is interesting to consider the energies of the absorption maxima above threshold in relation to the associated core level binding energies. The O 1s and Cu $2p_{3/2}$ core lines for Cu_2O in X-ray photoemission are shown in figure 4. The full widths at half maximum heights for these core lines of 0.66 eV and 1.32 eV are very much lower than in previous work. The line-widths are however much bigger than the resolution of the XPS system and probably represent the intrinsic line-widths determined by phonon and lifetime broadening. The O 1s binding energy is found to be 530.5 eV and the Cu $2p_{3/2}$ binding energy 932.6 eV. These binding energies are both in good agreement with previous work[23] and are referenced to the Fermi energy. As shown in the bottom panel of figure 4 the valence band edge in XPS is ~0.4 eV below the Fermi level. Given that the bandgap is 2.2 eV (to the nearest 0.1 eV), the bottom of the conduction band is determined to be (2.2 – 0.4) eV = 1.8 eV above the Fermi level. The maximal amplitudes in the computed empty O 2p and Cu 3d partial densities of states are in turn found in the bandstructure calculations 2.2 eV and 1.7 eV respectively above the bottom of the conduction band. Thus the peak maxima in the absorption spectra are expected at (530.5 + 1.8 + 2.2) eV = 534.5 eV for the O K edge and at (932.6 + 1.8 + 1.7) eV = 936.1 eV Cu L_3 edges. The actual maxima are found at 532.4 eV and

933.75 eV, representing downward shifts of 2.1 eV for the O K spectrum and 2.35 eV for the Cu L_3 spectrum. These energies are shown in figure 5. The shifts must be attributed to the effects of the core-hole potential as discussed earlier by Grioni *et al.*[25] The peak maximum in the Cu L_3 absorption spectrum lies 0.65 eV below the bottom of the conduction band (figure 5) and therefore corresponds to a true split-off core-hole exciton. By contrast the peak maximum in the O K absorption spectrum is 0.1 eV above the conduction band minimum and therefore corresponds to an excitonic resonance embedded in the conduction band.

D. Inelastic X-ray scattering

O K X-ray emission spectra of Cu_2O excited at the range of photon energies depicted in figure 3 are shown in figure 6. There is little change in the spectra with varying photon energy and in all cases the spectra seem to be dominated by the occupied O 2p partial density of states. By contrast there is a clear variation in the energy of spectral emission structure with exciting photon energy in the range between $h\nu$ = 931.50 eV and $h\nu$ = 933.75 eV for the Cu L_3 emission spectra shown in figure 7. When the spectra are transposed onto an energy loss scale it is seen that a feature at a constant energy loss of 4.5 eV appears over the photon energy range 931.5 eV < $h\nu$ < 933.75 eV. Above 933.75 eV the spectra evolve toward the non-resonant spectrum discussed previously, with the appearance of distinct shoulders on both the low and high energy sides of the main peak.

The loss structure near to threshold is interpreted in terms of interband excitations in Cu_2O. Following Kotani and Shin[55] and Jiménez-Mier *et al.*[56], the intensity of inelastically scattered photons at energy ω for incident energy Ω may be written in terms of filled and empty partial densities of states ρ_m and ρ_n:

$$F(\Omega,\omega) \propto \sum_{m,n} \left| \left\langle \phi_{Cu2p} \middle| t \middle| \phi_m \right\rangle \left\langle \phi_{Cu2p} \middle| t \middle| \phi_n \right\rangle \right|^2 \int \frac{\rho_m(\varepsilon)\rho_n'(\varepsilon + \Omega - \omega)}{(\varepsilon - \varepsilon_{Cu_{2p}} - \omega)^2 + \Gamma^2} d\varepsilon \qquad (1)$$

where t is a dipole operator acting between Cu 2p core states and valence and conduction band states ϕ_m and ϕ_n of appropriate symmetry and Γ represents the broadening due to the core hole. Since both Cu 2p to Cu 3d and Cu 2p to Cu 4s matrix elements are non-zero, the summation should include the four possible convolutions between the occupied and empty Cu 3d and 4s partial densities of states corresponding to the allowed channels in electronic Raman scattering where $\Delta l = 0$ or $\Delta l = \pm 2$ i.e. the summation should include the integrals involving $\rho_{Cu3d}\rho'_{Cu3d}$, $\rho_{Cu3d}\rho'_{Cu4s}$, $\rho_{4s}\rho'_{Cu3d}$ and $\rho_{Cu4s}\rho'_{Cu4s}$. We have evaluated the four energy-weighted convolutions given in expression (1) and these are shown in figure 8. Finally we computed a theoretical resonant inelastic X-ray scattering spectrum (RIXS) by weighting squares of matrix elements involving Cu 4s states by a factor of 1/10 as compared to those involving Cu 3d states. The results of this computation are also shown in figure 8, along with an experimental loss spectrum. Although the basic shape of the computed spectral profile is similar to that observed experimentally, the maximum in the experimental spectrum is about almost 2 eV lower in energy than calculated. This is despite the agreement between experimental and theoretical bandgaps. We attribute this discrepancy to excitonic effects. In fact the shift in the emission spectrum is very close to the shift in the absorption spectrum associated with the core hole potential. This observation has prompted us to adopt an *ad hoc* procedure for calculation of the inelastic loss spectrum in which the empty density of states from the bandstructure calculation in equation (1) is replaced by what we might call an excitonic density of states derived from experimental X-ray

absorption spectrum. As shown in figure 8 with this approach there is better agreement between observed and calculated spectra. Proper justification of the procedure is however problematic: the excitonic nature of the L shell X-ray absorption spectrum depends on the presence of the Cu 2p core hole, but in the RIXS final state there is obviously no core hole. In general RIXS spectra have in the past been found to be relatively insensitive to core-hole effects for simple materials such as graphite and c- and h-BN, where the main effect is to produce a redistribution of spectral weight.[57-61] On the other hand electron-valence hole interactions in the final state are known to enhance spectral weight at higher emission energies i.e. at lower loss energies, as is observed here. The valence electron exciton binding energy in Cu_2O is only about 0.14 eV.[62,63] However, the influence of final state exciton binding on the RIXS spectra may be amplified by localisation of the conduction band electron by the core hole in the intermediate state.[55] A fuller treatment of this problem will be presented elsewhere.

It is finally interesting to note that the lowest photon energy for which there is no longer evidence of loss structure is 934.75 eV, which is sufficient to promote an L_3 electron into the conduction band. In other words the range of photon energies under which inelastic X-ray scattering is observed are all in the excitonic regime.

V. CONCLUDING REMARKS.

First principles calculations on Cu_2O using a hybrid exchange approximation to density functional theory show that there is pronounced mixing between Cu 3d and O 2p states and that along with strong onsite hybridisation between Cu $3d_{z^2}$ and Cu 4s states, this mixing introduces

significant Cu 3d character into the conduction band of this oxide. Valence level photoemission spectroscopy in combination with O K shell and Cu L shell X-ray emission confirms that there is indeed pronounced cation-anion hybridisation.

Well-defined features are observed at a loss energy of 4.5 eV in resonant inelastic scattering close to the Cu 2p core threshold. To date most previous experimental works on resonant inelastic X-ray scattering of Cu compounds at the L edge has concentrated on open shell Cu(II) species[64], including CuO[65] and layered cuprates such as La_2CuO_4[65-67], $Sr_2CuO_2Cl_2$[67], $Bi_2Sr_2CaCu_2O_{8+\delta}$[67] and $Tl_2Ba_2CaCu_2O_8$.[68] Here the loss structure is typically found between 1.5 eV and 2.0 eV to low energy of the incident photon energy and can be understood in terms of localised excitations within the 3d manifold of energy levels, which are split by the ligand field.[61,67] The excitations found in the present work are at much higher loss energy and cannot be associated with ligand field excitations in the conventional sense because Cu_2O is a closed shell material. In the ionic limit the interband excitations we have observed could be described as 3d to 4s transitions. However onsite Cu $3d_{z^2}$ – Cu 4s hybridisation introduces significant Cu 3d character into the conduction band and the much bigger dipole matrix elements between core Cu 2p states and Cu 3d states as compared to Cu 2p to Cu 4s matrix elements means that the observed inelastic scattering is dominated by a convolution between the full and empty Cu 3d partial density of states. Similar resoant XES structure to that found here has been observed in RIX spectra of $CuAlO_2$[69] where a pronounced energy loss feature is found at 5.4 eV for excitation energies close to the L_3 core threshold. $CuAlO_2$ is another Cu(I) compound with linear coordination of Cu by two oxygen nearest neighbours. The similarity between the loss spectra in the two materials suggests that on-site interband excitations may be a general feature of RIX spectra of Cu(I) $3d^{10}$ materials.

Acknowledgements

Computer resources on the HPCx service were provided via our membership of the UK's HPC Materials Chemistry Consortium and funded by EPSRC (portfolio grant EP/D504872). Experimental work on transparent conducting oxides in Oxford is supported under EPSRC grant GR/S94148 and the NCESS Facility by Grant Scienta XPS facility by EPSRC grant EP/E025722/1. The Boston University program is supported in part by the U.S. Department of Energy under DE-FG02-98ER45680 and in part by the Donors of the American Chemical Society Petroleum Research Fund. The Advanced Light Source is supported by the Director, Office of Science, Office of Basic Energy Sciences, of the U.S. Department of Energy under Contract No. DE-AC02-05CH11231.

References

1. e.g. for a discussion of n-type doping in In_2O_3 see C. G. Granqvist and A. Hultåker, Thin Solid Films, **411 ,** 1 (2002)
2. T. Yamamoto and H.K. Yoshida, Jap. J. Appl. Phys., **38**, L166 (1999)
3. M. Joseph, H. Tabata and T. Kawai, Jap. J. Appl. Phys., **38**, L1205 (1999)
4. A. Tsukazaki, A. Ohtomo, T. Onuma, M. Ohtani, T. Makino, M. Sumiya, K. Ohtani, S.F. Chichibu, S. Fuke, Y. Segawa, H. Ohno, H. Koinuma and M. Kawasaki Nature Materials **4**, 42 (2005).
5. S. Nikitine, J.B. Grun and M. Sieskind, J. Phys. Chem. Solids, **17**, 292 (1961).
6. H. Kawazoe, M. Yasukawa, H. Hyodo, M. Kurita, H.M. Yanagi H, and H. Hosono Nature, **389,** 939 (1997).
7. H. Yanagi, S. Inoue, K. Ueda, H. Kawazoe, H. Hosono and N.Hamada, J. Appl. Phys., **88**, 4159 (2000).
8. K. Ueda, T. Hase, H. Yanagi, H. Kawazoe, H. Hosono, H. Ohta, M. Orita and M. Hirano, J. Appl. Phys., **89**, 1790 (2001).
9. H. Yanagi, H. Kawazoe, A. Kudo, M. Yasukawa and H. Hosono, Journal of Electroceramics **4**, 407 (2000).
10. H. Yanagi, T. Hase, S. Ibuki, K. Ueda and H. Hosono, Appl. Phys. Lett., **78**, 1583 (2001).
11. X.L. Nie, S.H. Wei and S.B. Zhang, Phys. Rev. Lett., **88**, 066405 (2002).
12. A. Kudo, H. Yanagi, H. Hosono and H. Kawazoe, Appl. Phys. Lett., **73**, 220 (1998).
13. H. Ohta, M. Orita, M. Hirano, I. Yagi, K. Ueda and H. Hosono, J. Appl. Phys., **91**, 3074 (2002).

14. S.N. Kale, S.B. Ogale, S.R. Shinde, M. Sahasrabuddhe, V.N. Kulkarni, R.L. Greene and T. Venkatesan, Appl. Phys. Lett., **82**, 2100 (2003)

15. M. Ivill, M.E. Overberg, C.R. Abernathy, D.P. Norton, A.F. Hebard, N. Theodoropoulou, and J.D. Budai, Solid State Electronics, **47**, 2215 (2003).

16. M. Wei, N. Braddon, D. Zhi, P.A. Midgley, S.K. Chen, M.G. Blamire, J.L. MacManus-Driscoll. Appl. Phys. Lett., **86**, 072514 (2005)

17. L.Q. Pan, H. Zhu, C.F. Fan, W.G. Wang, Y. Zhang and J.Q. Xiao, J. Appl. Phys. **97**, 10D318 (2005)

18. J. Drahokoupil, M. Polcik and E. Pollert, Solid State Commun., **66**, 4(1988)

19. J. Drahokoupil, M. Polcik and E. Pollert, Solid State Commun., **74**, 8 (1990)

20. D.R. Mueller, J. Wallace, D.L. Ederer, J.J. Jia, W.L. O'Brien, Q.Y. Dong and T.A. Callcott, Phys. Rev. B, **46**, 11069 (1992).

21. J.M. Mariot, V. Branole, C.F. Hague, G. Vetter and F. Queyroux, Z. Phys. B, **75**, 1 (1989).

22. G.K. Wertheim and S. Hüfner, Phys. Rev. Lett., *20*, 1028 (1972)

23. J. Ghijsen, L.H. Tjeng, J. vanElp, H. Eskes, J. Westerink, G.A. Sawatzky and M.T. Czyzyk, Phys. Rev. B, **38**, 11322 (1988)

24. S.L. Hulbert, B.A. Bunker, F.C. Brown and P. Pianetta, Phys. Rev. B, **30**, 2120 (1984)

25. M. Grioni, J.F. van Acker, M.T. Czyzyk and J.C. Fuggle, Phys. Rev. B, **45**, 3309 (1992)

26. M. Grioni, J.B. Goedkoop, R. Schoorl, F.M.F. deGroot, J.C. Fuggle, F. Schafers, E.E. Koch, G. Rossi, J.M. Esteva and R.C. Karnatak, Phys. Rev. B, **39**, 1541 (1989).

27. A.F. Wells, *Structural Inorganic Chemistry*, (Clarendon Press, Oxford, 1984)

28. R. Mittal, S.L. Chaplot, S.K. Mishra and P.P. Bose, Phys. Rev. B, **75**, 174303 (2007)

29. U. Fano and J.W. Cooper, Rev. Mod. Phys., **40**, 441 (1968).

30. R. Dovesi, V.R. Saunders C. Roetti, R. Orlando, C.M. Zicovich-Wilson, F. Pascale, B. Civalleri, K. Doll, N.M. Harrison, I.J. Bush, Ph. D'Arco, M. Llunell CRYSTAL06 User's Manual, University of Torino, Torino, 2006
31. X-B. Feng and N. M. Harrison, Phys. Rev. B, **69**, 132502 (2004)
32. J. Muscat, A. Wander, N. M. Harrison, Chem. Phys. Lett., **342,** 397 (2001)
33. K. Doll, N. M. Harrison 2000, Chem. Phys. Letters, **317**, 282 (2000)
34. M .I. McCarthy, N.M. Harrison, Phys. Rev. B, **49**, 8574 (1994)
35. K.H. Schultz and D.F. Cox, Phys. Rev. B, **43**, 1610 (1990)
36. D.F. Cox and K.H. Schultz, Surf. Sci., **249**, 138 (1991).
37. D.F. Cox and K.H. Schultz, Surf. Sci., **256**, 67 (1991).
38. Practical Surface Analysis, ed. D. Briggs and M.P. Seah, Wiley, Chichester (1990).
39. J. Nordgren and R. Nyholm, Nucl. Instrum. Methods, A **246**, 242 (1986).
40. J. Nordgren, G. Bray, S. Cramm, R. Nyholm, J.E. Rubensson, and N. Wassdahl, Rev. Sci. Instrum. **60**, 1690 (1989).
41. J. P. Dahl and A.C. Switendick, J. Phys. Chem. Solids, **27**, 931 (1966).
42. L. Kleinman and K. Mednick, Phys. Rev. B, **21**, 1549 (1980)
43. J. Robertson, Phys. Rev. B, **28**, 3378 (1983)
44. P. Marksteiner, P. Blaha and K. Schwarz, Z. Phys. B, **64**, 119 (1986)
45. E. Ruiz, S Alvarez, P. Alemany and R.A. Evarestov, Phys. Rev. B, **56**, 7189 (1997)
46. A. Martinez-Ruiz, M. G. Moreno and N. Takeuchi, Solid State Sciences, **5**, 291 (2003)
47. X. Nie, S.-H. Wei and S.B. Zhang, Phys. Rev. B, **65**, 075111 (2002)
48. A. Filippetti and V. Fiorentini, Phys. Rev. B, 72, 035128 (2005)
49. M. Nolan and S.D. Elliot, Phys. Chem. Chem. Phys., **8**, 5350 (2006)
50. Y. Dou, R.G. Egdell, D.S.L. Law, N.M. Harrison and B.G. Searle

J. Phys.Condens. Matter, **10,** 8447 (1998)

51. L.E. Orgel, J. Chem. Soc., 4186 (1958)
52. A. Önsten, M.Mansson, T. Claesson, T. Muro, T. Matsushita, T. Nakamura, T. Kinoshita, U.O. Karlsson and O. Tjernberg, Phys. Rev. B, **76**, 115127 (2007)
53. us CPL
54. J. J. Yeh and I. Lindau, At. Data Nucl. Data Tables, **32** , 1 (1985)
55. A. Kotani and S. Shin, Rev. Mod. Phys., **73**, 203 (2001).
56. J. Jiménez-Mier, J. van Ek, D.L. Ederer, T.A. Callcott, J.J. Jia, J. Carlisle, L. Terminello, A. Asfaw and R.C. Perera, Phys. Rev. B, **59**, 2649 (1999).
57. E.L. Shirley, Phys. Rev. Lett., **80**, 794 (1998).
58. E.L. Shirley, J.A. Soininen, G.P. Zhang, J.A. Carlisle, T.A. Callcott, D.L. Ederer, L.J. Terminello and R.C. Perera, J. Electron Spectrosc. Relat. Phenom., **114-116**, 939 (2001).
59. T. Minami and K. Nasu, J. Electron Spectrosc. Relat. Phenom., **92**, 231 (1998)
60. M. vanVeenendaal and P. Carra, Phys. Rev. Lett., **78**, 2839 (1997)
61. T. Minami, J. Phys. Soc. Jpn., **67**, 3598 (1998).
62. V.T. Agekyan, Phys. Stat. Solidi A, **43**, 11 (1977)
63. D.P. Trauernicht, J.P. Wolfe and A. Mysyrowicz, Phys. Rev. Lett., **52**, 855 (1984).
64. S. Tanaka and A. Kotani, J. Phys. Soc. Jpn., **62,** 464 (1993).
65. K. Ichikawa, K. Jouda, S. Tanaka, K. Soda, M. Matsumoto, Y. Taguchi, T. Katsumi, O. Aita, H. Maezawa, Y. Azuma and H. Kitzawa, J. Electron Spectrosc. Relat. Phenom., **78**, 183 (1996)
66. L.C. Duda, G. Dräger, S. Tanaka, A. Kotani, J. Guo, D. Heumann, S. Bocharov, N. Wassdahl and J. Nordgren, J. Phys. Soc. Jpn., **67**, 416 (1998)
67. G. Ghiringhelli, N.B. Brookes, E. Annese, H.Berger, C. Dallera, M. Grioni, L. Perfetti, A. Tagliaferri and L. Braicovich, Phys. Rev. Lett., **92,** 117406 (2004).

68. W.A. Little, M.J. Holcomb, G. Ghiringhelli, L. Braicovich, C. Dallera, A. Piazzalunga, A. Tagliaferri and N.B. Brookes, Physica C, **460-462,** 40 (2007).

69. D. J. Aston, D. J. Payne, A. J. H. Green, R. G. Egdell, D. S. L. Law, J. Guo, P. A. Glans, T. Learmonth and K. E. Smith, Phys. Rev. B, **72,** 195115 (2005)

Table 1. Bandgaps and valence band width in Cu_2O from bandstructure calculations compared with experimental data.

Reference	Technique	Bandgap (eV)	Valence band width (eV)
42	Self consistent LDA[a] with localised Gaussian basis and Slater exchange	1.1	6.0
43	Parameterised semi-empirical tight binding	2.2	8.2
44	LAPW[b]	~0.6	6.8
45	Hartree-Fock with DFT[c] correction	9.7	7.0
46	GGA FP-LAPW[d] (WIEN97)	~0.5	7.2
47	LDA GP-LAPW	0.52	7.2
48	LDA	0.55	7.5
	LDA with SIC	1.80	8.2
49	DFT	~0.5	7.5
5	Experimental	2.17	-
Present	Hybrid exchange DFT[c]	2.1	7.8
Present	Experimental	-	~8.0

[a] Local density approximation

[b] Linear augmented plane wave

[c] Density functional theory

[d] Generalised gradient approximation full potential linear augmented plane wave

[e] General potential linearised augmented plane wave

Captions for figures.

Figure 1.

Full and partial densities of states for Cu_2O derived from bandstructure calculations.

Figure 2.

Left hand panels: Al Kα excited valence band X-ray photoemission and non-resonant Cu L_3 and O-K X-ray emission spectra of Cu_2O. Right hand panels: cross section weighted density of states and Cu 3d and O 2p partial densities of states for Cu_2O appropriately broadened.

Figure 3.

Solid lines: X-ray absorption spectra for Cu_2O measured close to the O K and Cu L edges in the total fluorescence yield mode. Dotted line: as above but measured in total electron yield mode. Dashed lines: empty O 2p and Cu 3d partial densities of states from bandstructure calculations. The diamonds indicate the energies at which X-ray emission spectra were excited.

Figure 4.

O1s and Cu $2p_{3/2}$ core Al Kα photoemission spectra of Cu_2O. Binding energies are referenced to the Fermi level. The valence band onset spectrum in the bottom level shows that the Fermi level is found 0.4 eV above the valence band maximum.

Figure 5

Schematic energy level diagram showing the relationship between energies in XPS, XAS and XES for O K and Cu L_3. The shaded region indicates the range of photon energies over which resonant inelastic scattering is observed at the Cu L_3 edge.

Figure 6.

O K X-ray emission spectra of Cu_2O excited over a range of photon energies close to threshold. The emission features show little change with changing photon energy.

Figure 7.

Upper panel: Cu L_3 X-ray emission spectra of Cu_2O excited over a range of photon energies close to threshold. The emission features show strong variation in energy for exciting photon energies closest to threshold between 931.50 eV and 934.75 eV. Lower panel: emission spectra as above but presented on an energy loss scale.

Figure 8.

Upper panel. Computed terms for the four dipole allowed channels included in the summation in equation (1). Lower panel. Dashed line: computed inelastic X-ray scattering spectrum, obtained by appropriately weighting the four channels shown above. Solid line: computed inelastic scattering spectrum using "excitonic" density of states. In all cases the simulated spectra have been broadened by a Gaussian with full width at half maximum height of 1.35 eV to include the effects of broadening of the core hole. Dotted line: experimental energy loss spectrum excited at $h\nu$ = 933.75 eV.

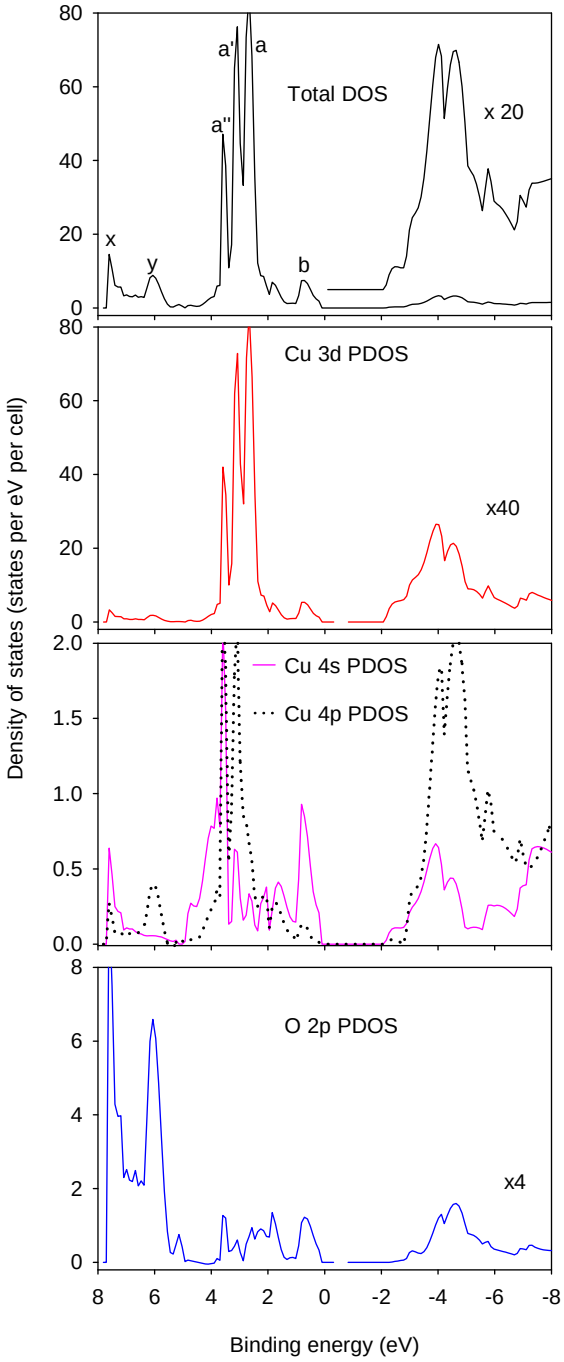

Total DOS
x 20
a'
a
a''
x
y
b
Cu 3d PDOS
x40
Cu 4s PDOS
Cu 4p PDOS
O 2p PDOS
x4
Density of states (states per eV per cell)
Binding energy (eV)

Figure 1

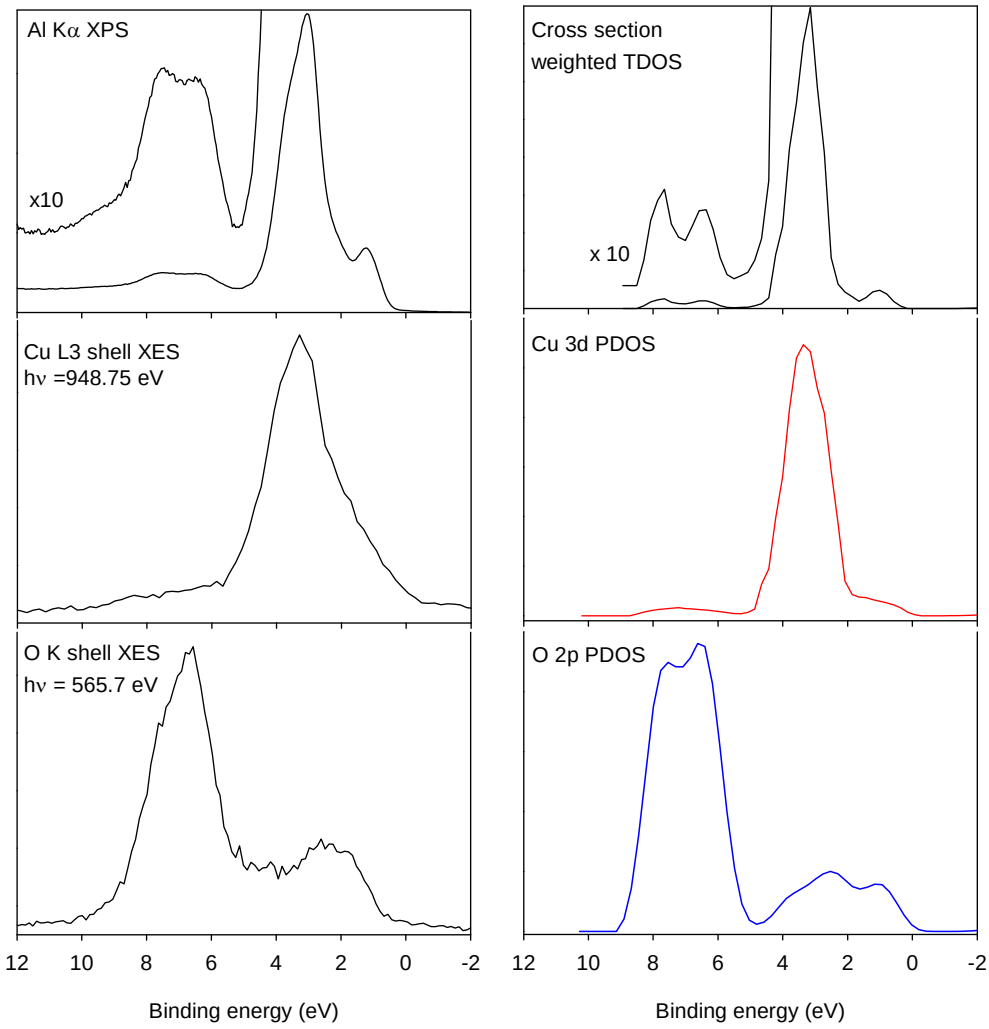

Al Kα XPS
x10
Cross section
weighted TDOS
x 10
Cu L3 shell XES
hν =948.75 eV
Cu 3d PDOS
O K shell XES
hν = 565.7 eV
O 2p PDOS
12 10 8 6 4 2 0 -2
Binding energy (eV)
12 10 8 6 4 2 0 -2
Binding energy (eV)

Figure 2

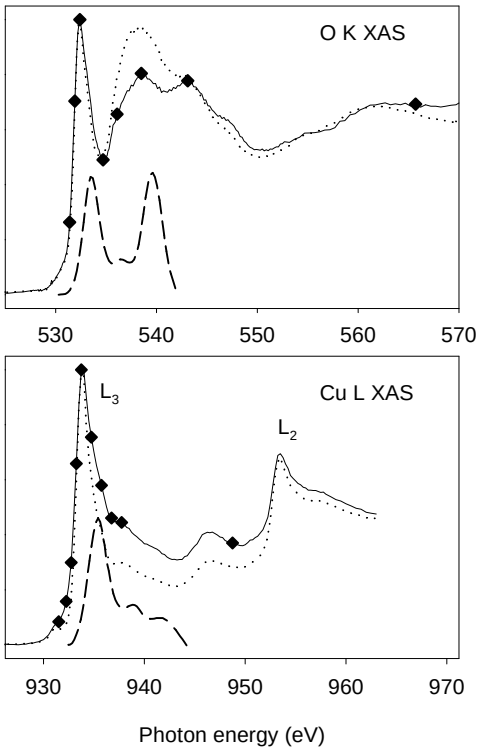

O K XAS
530
540
550
560
570
L3
L2
Cu L XAS
930
940
950
960
970
Photon energy (eV)

Figure 3

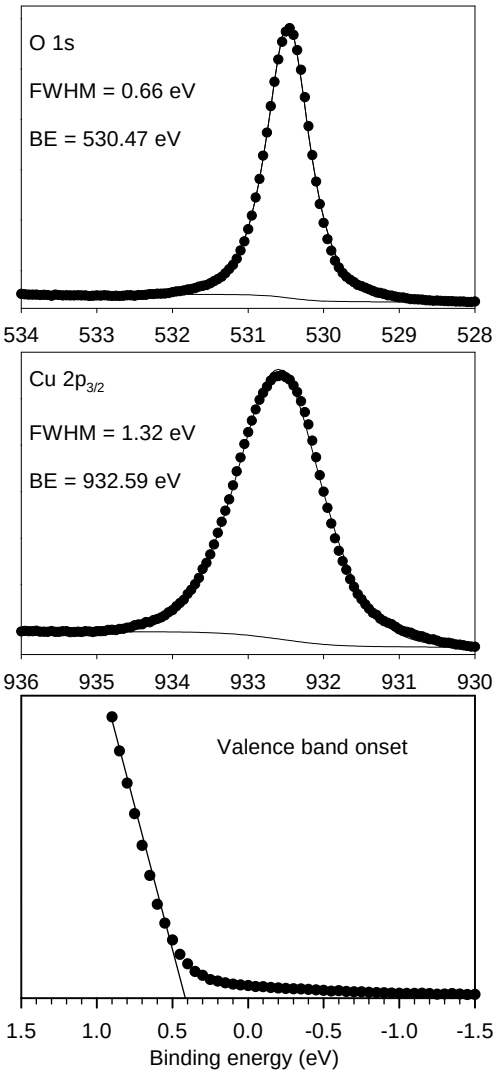

O 1s
FWHM = 0.66 eV
BE = 530.47 eV
534
533
532
531
530
529
528
Cu 2p3/2
FWHM = 1.32 eV
BE = 932.59 eV
936
935
934
933
932
931
930
Valence band onset
1.5
1.0
0.5
0.0
-0.5
-1.0
-1.5
Binding energy (eV)

Figure 4

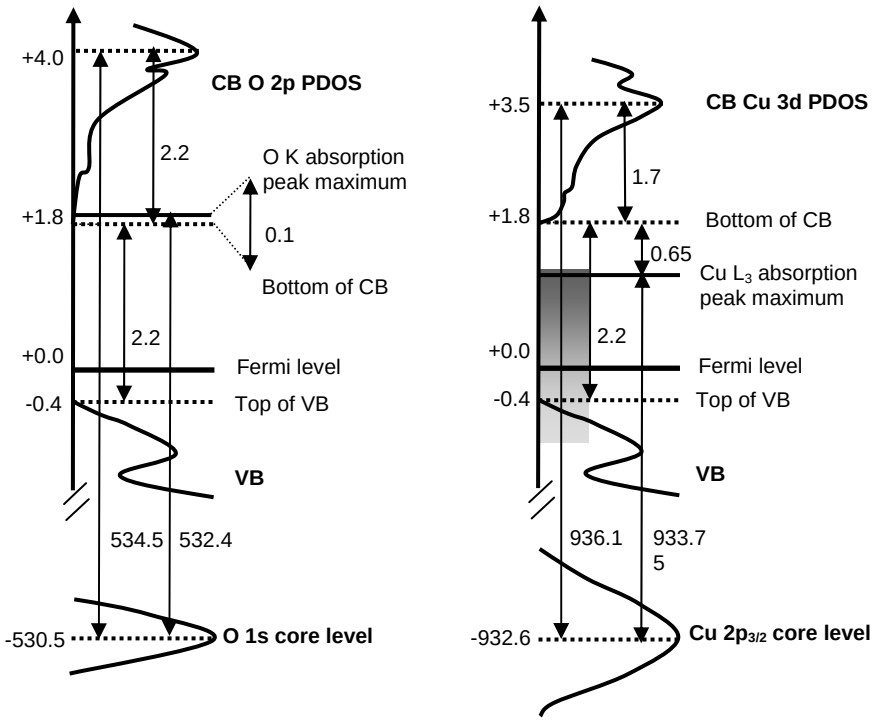

+4.0
CB O 2p PDOS
2.2
O K absorption
peak maximum
+1.8
0.1
Bottom of CB
2.2
+0.0
Fermi level
-0.4
Top of VB
VB
534.5
532.4
-530.5
O 1s core level
+3.5
CB Cu 3d PDOS
1.7
+1.8
Bottom of CB
0.65
Cu L3 absorption
peak maximum
2.2
+0.0
Fermi level
-0.4
Top of VB
VB
936.1
933.7
5
-932.6
Cu 2p3/2 core level

Figure 5

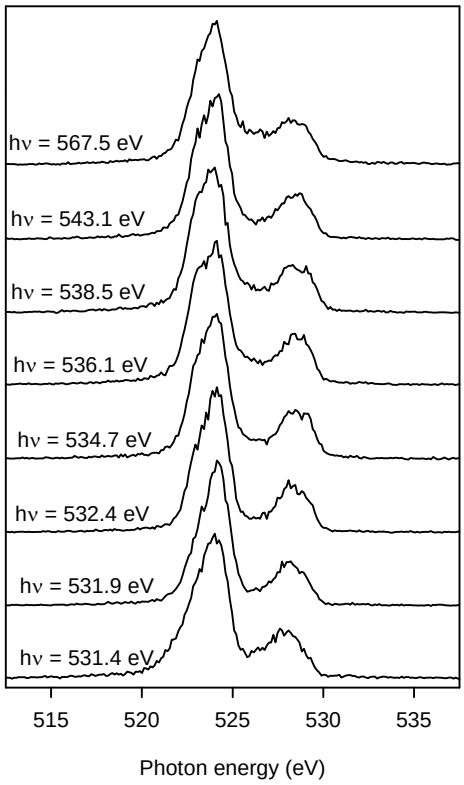

hν = 567.5 eV
hν = 543.1 eV
hν = 538.5 eV
hν = 536.1 eV
hν = 534.7 eV
hν = 532.4 eV
hν = 531.9 eV
hν = 531.4 eV
515
520
525
530
535
Photon energy (eV)

Figure 6

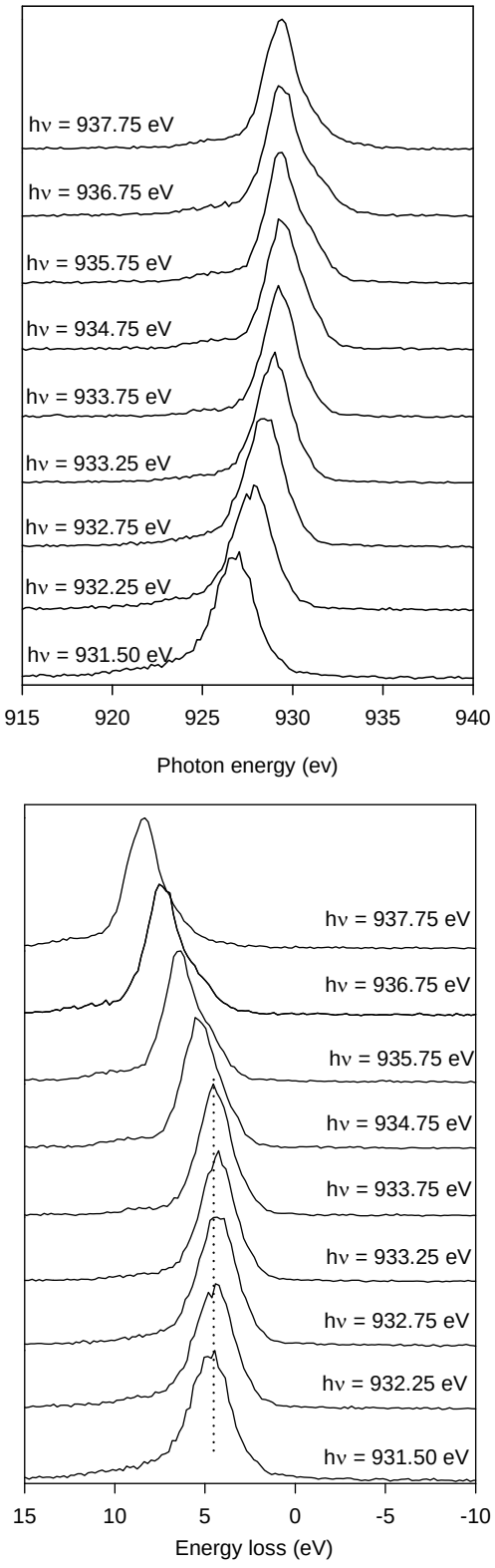

hν = 937.75 eV
hν = 936.75 eV
hν = 935.75 eV
hν = 934.75 eV
hν = 933.75 eV
hν = 933.25 eV
hν = 932.75 eV
hν = 932.25 eV
hν = 931.50 eV
915
920
925
930
935
940
Photon energy (ev)
hν = 937.75 eV
hν = 936.75 eV
hν = 935.75 eV
hν = 934.75 eV
hν = 933.75 eV
hν = 933.25 eV
hν = 932.75 eV
hν = 932.25 eV
hν = 931.50 eV
15
10
5
0
-5
-10
Energy loss (eV)

Figure 7

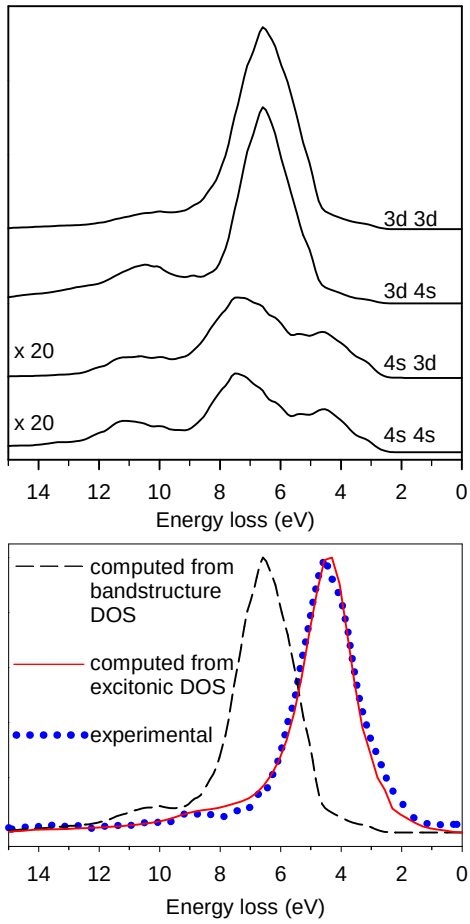

3d 3d
3d 4s
x 20
4s 3d
x 20
4s 4s
14
12
10
8
6
4
2
0
Energy loss (eV)
computed from bandstructure DOS
computed from excitonic DOS
experimental
14
12
10
8
6
4
2
0
Energy loss (eV)

Figure 8